

Supplementary Materials for

Infrared vibrational nano-crystallography and nano-imaging

Eric A. Muller, Benjamin Pollard, Hans A. Bechtel, Peter van Blerkom, Markus B. Raschke

Published 7 October 2016, *Sci. Adv.* **2**, e1601006 (2016)

DOI: 10.1126/sciadv.1601006

This PDF file includes:

- Description of modeling and calculations for IR vibrational nano-crystallography
- Description of nonresonant signal and signal penetration depth
- fig. S1. Experiment and calculated near- and far-field spectra.
- fig. S2. Orientation dependence of near-field signal.
- fig. S3. Nonresonant near-field signal.

Supplementary Materials

We discuss below details of the model for infrared optical nano-crystallography. The model is built on a Lorentzian oscillator model using measured relative oscillator strengths, which are then included in the *s*-SNOM response using the spherical dipole model. We then discuss further details of both broadband SINS and single-wavelength *s*-SNOM, and non-resonant contributions to the observed *s*-SNOM signal.

Model for Infrared Nano-Crystallography

In order to determine oscillator strength of vibrational modes, we first measure the FTIR transmission spectra of PTCDA powder prepared by pressing in a KBr pellet, as shown in fig. S1a. Powder is isotropically dispersed in the pellet such that the projection of the transition dipole moment of each vibrational mode contributes equally, $\langle \cos^2(\theta) \rangle = 1/2$, to an orientationally averaged spectrum. We fit the spectrum to a sum of Lorentzians, leaving the frequency and line width of modes as constants from previously reported investigations (37). The fits to relative oscillator strengths of the vibrational modes in our spectra match measurement well within reported uncertainty (37).

We assign vibrational peaks based upon previously reported normal modes and symmetries (36). PTCDA molecules crystallize in the monoclinic structure with D_2h symmetry. The *C-H* out-of-plane modes have B_3u symmetry with transition dipole along the crystalline *a*-axis. The *C=O* modes have B_u and B_2u symmetry with transmission dipoles along the *b*- and *c*-axes, which cannot be further distinguished due to the herringbone structure.

We then calculate the orientation-dependent optical response with a Lorentzian oscillator model. The frequency dependent infrared dielectric constant $\epsilon_{sample}(\bar{\nu})$ can be expressed as the sum of individual molecular vibrations (equation S1)

$$\epsilon(\bar{\nu}) = \epsilon_0 + \sum_j N/V \cdot \cos^2\left(\frac{\delta\mu_\alpha^j}{\delta Q_j}\right) \frac{\bar{\nu}_j^2}{\bar{\nu}_j^2 - \bar{\nu}^2 - 2i\bar{\nu}\gamma_j}$$

for a material with density N/V and zero-frequency dielectric constant ϵ_0 . Each vibrational mode j with transition dipole $\delta\mu_\alpha^j / \delta Q_j$ contributes Lorentzian response with center frequency $\bar{\nu}_j$ and damping coefficient γ_j (15, 37). The orientation-dependence of $\epsilon_{sample}(\bar{\nu})$ results from the projection angle θ_j of each $\delta\mu_\alpha^j / \delta Q_j$ in the direction the *z* axis probed by the near-field of the *s*-SNOM tip. Finally, we apply the generalized orientation-dependent model for $\epsilon_{sample}(\bar{\nu})$ to PTCDA using the oscillator strengths and symmetry assignments from above.

We model the tip interaction using the spherical dipole model, which approximates the AFM tip (38). The polarizability of a tip with radius R and dielectric constant ϵ_{tip} is given by the Clausius-Mossetti equation $\alpha_{sph} = 4\pi R^3 (\epsilon_{tip} - 1) / (\epsilon_{tip} + 2)$. The scattered signal from the near-field is then proportional to the effective polarizability of the tip and sample (equation S2)

$$\alpha_{eff} = \alpha_{sph} \left[1 - \frac{\alpha_{sph}}{16\pi(R_t + z)^3} \frac{\epsilon_{sample} - 1}{\epsilon_{sample} + 1} \right]^{-1}$$

for a height z above the sample. Combining equation S2 with $\epsilon_{sample}(\nu)$ from equation S1 results in a model for the infrared s -SNOM signal as a function of molecular and crystalline orientation. We note that the spherical dipole model is known to have limitations for accurately fitting peak shapes for strong oscillators, and several more complex models have been developed (39, 40). We find that in the case of PTCDA, line shapes can be adequately fit accurately within our spectral resolution using the spherical dipole model. The model overestimates the spectral blue shift that occurs with increasing resonant vibrational response by as much as 4 cm^{-1} for the $C=O$ stretch, however this is small compared to both the full width at half maximum of $\Phi_{NF}(\bar{\nu})$ (25 cm^{-1}) and the spectral resolution of the measurement (8 cm^{-1}) (41).

Broadband and Selected-Frequency s -SNOM Implementation

Figure S1b shows the $A_{NF}(\bar{\nu})$ and $\Phi_{NF}(\bar{\nu})$ from two different nanoscale regions. The spectra in fig. S1b show a frequency range, with the zoomed in spectra shown in Fig. 2. We fit these SINS spectra using our orientation-dependent s -SNOM model using θ as a free fitting parameter and, treating the peak positions, line widths, and oscillator strengths as constants. The calculated $A_{NF}(\bar{\nu})$ and $\Phi_{NF}(\bar{\nu})$ from the spherical dipole model fit well to experimental SINS spectra, we see good agreement with peak position, line width and relative oscillator strength for a given θ . A significant deviation in the baseline is observed near 1100 cm^{-1} , however, which we attribute to imperfect background subtraction of the vibrational signature of polydimethylsiloxane, which is a well-known contaminant on commercial AFM tips. The spectral regions containing the $C-H$ and $C=O$ modes are observed to be relatively free from interference.

The measured Φ_{NF} at a selected frequency resonant with a vibration mode can be used to determine θ . Figure S2a shows zoomed-in regions of the SINS spectra shown in fig. S1b containing only the four $C=O$ stretching modes. As shown in fig. S2b, we observe quantitative agreement between model and experiment for the Φ_{NF} on resonance with the $C=O$, spectral line shape, and mode splitting as a function of projection angle θ . Repeated SINS spectra demonstrate that $\Phi_{NF}(C=O)$ are reproducible with little interference from extrinsic factors. From this, we can calculate the expected Φ_{NF} versus θ for selected optical frequencies resonant with particular vibrational modes as shown in fig. S2c. We can then utilize the angle dependence to enable quantitative measurement of θ for PTCDA thin films with selected frequency IR s -SNOM imaging.

Although the imaginary component of the *s*-SNOM signal is also often used because the line shape more closely resembles far-field FTIR transmission, it is reported in arbitrary units of instrument response, preventing quantitative analysis of peak heights. We use $\Phi_{NF}(\nu)$ in order to compare calculated spectra with *s*-SNOM signal from both broadband spectra and single-wavelength images.

Non-Resonant *s*-SNOM of PTCDA

Finally, we compare resonant and non-resonant *s*-SNOM signal. Figure S3a shows the AFM topography at a location near the edge, from the same region shown in Fig. 3A. The corresponding resonant $\Phi_{NF}(1777\text{cm}^{-1})$ shown in Fig. 3B measures variation in θ across the PTCDA film. The non-resonant $\Phi_{NF}(1701\text{cm}^{-1})$ shown in fig. S2b, however, shows little variation across the image. The off-resonant $\Phi_{NF}(1701\text{cm}^{-1})$ contains no information on *C=O* vibrational modes and the small image contrast can be attributed to the non-resonant tails of nearby vibrational modes. We calculate uncertainty in the selected-frequency spectra from noise in the $\Phi_{NF}(1701\text{cm}^{-1})$ image. The standard deviation of $\Phi_{NF}(1701\text{cm}^{-1})$ in the image is 4° , which corresponds to a two sigma uncertainty in crystalline orientation of $\theta = \pm 10^\circ$.

Figure S3c shows a map of $A_{NF}(1701\text{cm}^{-1})$. The $A_{NF}(\bar{\nu})$ signal results primarily from the real part of the sample dielectric constant without resonance information. The PTCDA region shows a lower signal than the Au because of the correspondingly lower dielectric constant. We perform correlation analysis of both $A_{NF}(1701\text{cm}^{-1})$ and $A_{NF}(1777\text{cm}^{-1})$ versus height (fig. S3d). The resulting correlation plot of $A_{NF}(\bar{\nu})$ shows a monotonically decaying signal versus height. At low heights, the signal corresponds to bare Au, and the signal with large heights corresponds to thick regions of PTCDA. The monotonically decaying signal versus thickness results from the finite penetration depth of the *s*-SNOM near-field, with a penetration depth of $\sim 30\text{-nm}$. No distinct sub-populations are observed in correlation plot of $A_{NF}(1701\text{cm}^{-1})$ or $A_{NF}(1777\text{cm}^{-1})$. This can be expected for a material with constant ϵ_0 and N/V , since orientation dependence is only observed through the resonant vibrational response.

Correlation analysis of non-resonant $\Phi_{NF}(1701\text{cm}^{-1})$ similarly shows a single population and contains no information related θ . Lack of distinct populations sub-ensemble in any non-resonant *s*-SNOM channels, $A_{NF}(1701\text{cm}^{-1})$, $A_{NF}(1777\text{cm}^{-1})$ or $\Phi_{NF}(1701\text{cm}^{-1})$, supports our interpretation and analysis of resonant $\Phi_{NF}(1777\text{cm}^{-1})$ for identification of spatially distinct sub-ensemble populations.

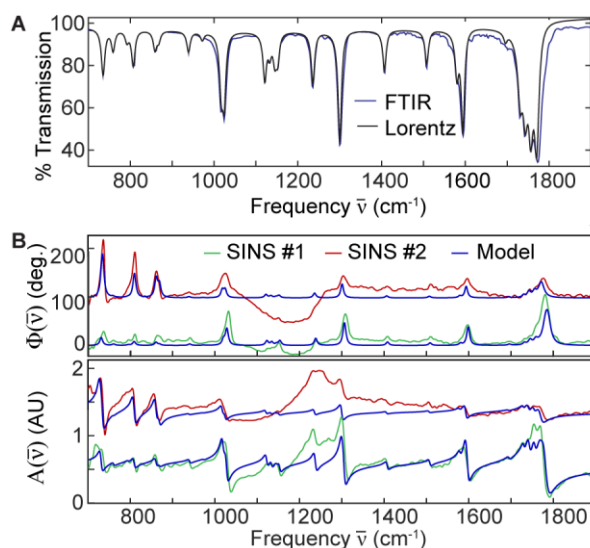


fig. S1. Experiment and calculated near- and far-field spectra. (a) Far-field FTIR transmission spectrum of PTCDA particles in KBr are fit to a Lorentzian oscillator model. (b) SINS spectra of PTCDA at two different regions (red and green, offset for clarity) with corresponding angle-dependent fit using the spherical dipole model for Lorentzian oscillators. Zoomed in spectra and angle assignments discussed in Fig. 2B.

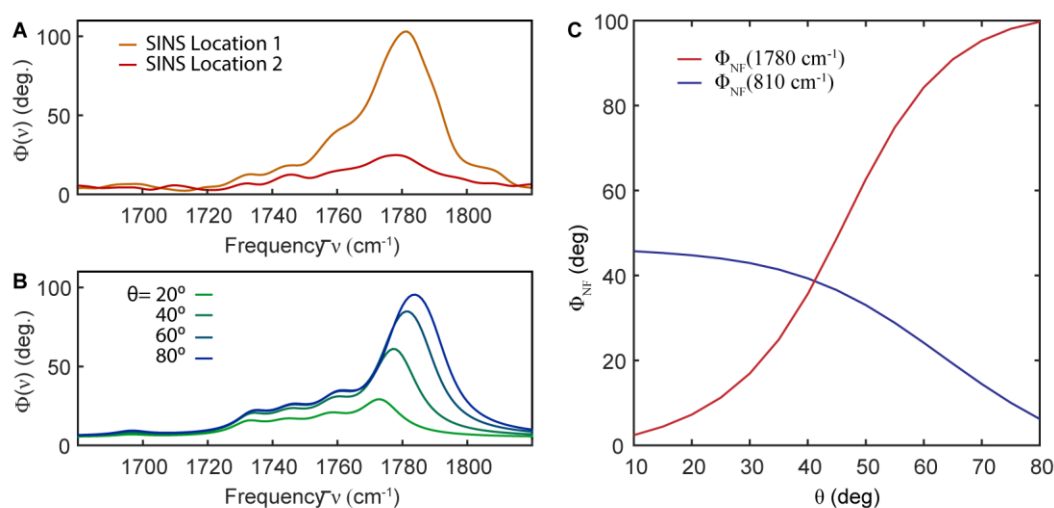


fig. S2. Orientation-dependence of near-field signal. SINS spectrum of PTCDA (a) dropcast particles and (b) molecular beam deposition showing the imaginary and real components of the σ -SNOM signal σ . (b) Modeled spectra are calculated using the orientation-dependent dielectric response function of PTCDA. (c) Calculated Φ_{NF} versus θ at two wavenumbers corresponding to the carbonyl and C-H out-of-plane vibrational resonances.

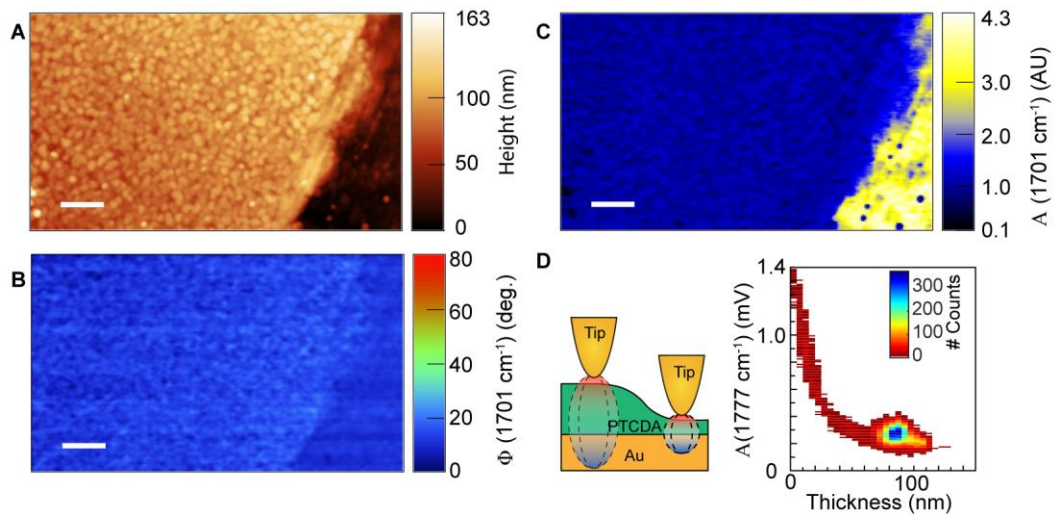


fig. S3. Nonresonant near-field signal. Vacuum deposited PTCDA near the film edge showing (a) AFM height, (b) non-resonant $\Phi_{NF}(1701\text{cm}^{-1})$, and (c) $A_{NF}(1701\text{cm}^{-1})$. (d) By scanning the AFM tip across different thicknesses of PTCDA (left) we construct a correlation plot $A(1777\text{cm}^{-1})$ versus PTCDA thickness. Scale bars 1 μm .